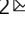**ARTICLE**

OPEN

Check for updates

Unbiased description of magnetic polarons in a Mott insulator

Emil Blomquist [1] & Johan Carlström [2✉]

Polarons are among the most elementary quasiparticles of interacting quantum matter, consisting of a charge carrier dressed by an excited background. In Mott insulators, they take the form of a dopant surrounded by a distorted spin-background. Despite the fundamental importance of polarons for the electronic structure of strongly correlated systems, access to their internal structure was only recently realized in experiments, while controllable theoretical results are still lacking due to the sign problem. Here we report unbiased high-precision data obtained from worm-algorithm Monte Carlo that reveal the real-space structure of a polaron in the *t-J* model deep inside the region where the sign problem becomes significant. These results are directly comparable to recent quantum gas microscopy experiments, but give access to significantly lower temperatures.

[1] Department of Physics, Royal Institute of Technology, Stockholm SE-106 91, Sweden. [2] Department of Physics, Stockholm University, Stockholm 106 91, Sweden. ✉email: johan.carlstrom@fysik.su.se

The doped Mott insulator with charge carriers that propagate on an antiferromagnetic background has been identified as the paradigmatic model of the high-temperature superconductors[1]. In this scenario, the dopants and the environment form composite polarons[2] as a result of competition between the kinetic energy and super-exchange processes in the background[3]. The carriers can lower their energy by delocalizing, but this is incompatible with anti-ferromagnetism as their motion disrupts the magnetic order. Retaining antiferromagnetic correlations minimizes the exchange energy, but this effectively leads to narrowing of the band due to a finite mean-free path[4]— delocalization of the carrier within a cloud of altered spin correlations results as a compromise. In doped Mott insulators, polarons are expected to dictate effective mass, transport properties and interactions between carriers[5–7].

Since the polaron is the elementary quasiparticle of the doped Mott insulator, it is also the starting point for understanding its electronic structure, including the enigmatic mechanism of high-temperature superconductivity. While still a matter of active research, the premise that the perturbed spin-background mediates attraction between carriers is considered to be central to the explanation of pairing[8,9]. Attraction between carriers in a Mott insulator is also indicated by density matrix renormalization group (DMRG) calculations[10].

Currently, to the best of our knowledge, no approximation-free theoretical results without systematic bias exist for the internal structure of the polaron. Exact diagonalization (ED) can resolve spin correlations in the vicinity of the carrier, but the restriction to small system sizes means that the polaron is distorted by boundary pressure. DMRG allows addressing larger systems than ED but is strictly speaking an approximative technique, albeit potentially very accurate[11]. Other approximative techniques include Monte Carlo based on spin-charge transformation and separation[12]. In macroscopic systems, the fermionic sign problem prevents the effective use of conventional quantum Monte Carlo techniques[13]. Diagrammatic simulation techniques can in principle be applied to correlated systems, but are currently limited to comparatively high temperatures[14,15].

Until recently, detailed information about polarons was equally unavailable in experiments, as electronic systems are generally not accessible to the required precision. With the advent of quantum gas microscopy, this has changed completely, and imaging of entangled quantum many-body states is now possible at the level of single-site resolution[16]. The experimental realization of strongly correlated systems in ultra-cold atomic gases has at this point reached temperature ranges where the Mott-insulating state develops antiferromagnetic correlations[17], and the first observation of the internal structure of a polaron in this setting was reported recently[18]. Per expectations, this experiment confirms that the carrier is dressed by local reduction, or even reversal, of spin correlations. A comparison to the case of a pinned dopant establishes that delocalization is essential to the structure of the polaron.

Worm-algorithm Monte Carlo (WAMC) provides an exceptionally efficient protocol for obtaining the statistical properties of quantum many-body systems at thermal equilibrium[19]. For bosonic systems, this technique allows computing unbiased and controllable results for strongly interacting systems at energy scales far below condensation[20]. For fermions, the sign problem limits the applicability to Gutzwiller-projected theories where sign fluctuations are only extensive in the number of carriers as opposed to system size. To date, this technique has been used to derive the spectral properties of a single carrier in the $t–J$ model[21], which transpires at imaginary timescales where the sign problem is manageable[22].

In this work, we employ WAMC to resolve the internal structure of a single polaron in the $t–J$ model. By relying on an efficient sampling protocol and large-scale simulations, we can extract accurate data deep into the temperature range where the sign problem becomes significant.

Results

Using WAMC, we obtain unbiased spin correlations in the proximity of the charge carrier that are directly comparable to experiments on ultra-cold atomic gases. Below, we outline how this technique is deployed, and discuss key observables.

Observables and model. We focus on observing real-space spin correlations, as these are also relevant for current experiments based on electron gas microscopy. In line with ref. [18], we consider correlators of the form

$$C_{|\mathbf{d}|}(\mathbf{r}) = 4\langle S^z_{\mathbf{r}_0+\mathbf{r}-\mathbf{d}/2} \, S^z_{\mathbf{r}_0+\mathbf{r}+\mathbf{d}/2}\rangle. \quad (1)$$

Here $\mathbf{r}_0$ and $\mathbf{r}_0 + \mathbf{r} \pm \mathbf{d}/2$ are the positions of the carrier and the two spins, respectively, while $\mathbf{r}$ defines the bond distance. We will consider only the cases $|\mathbf{d}| = 1$ (nearest neighbor), $|\mathbf{d}| = \sqrt{2}$ (next-nearest neighbor), and $|\mathbf{d}| = 2$ (next-next-nearest neighbor). The correlators are illustrated in Fig. 1.

The principal observables generated by WAMC are diagonal elements of the density matrix, from which we can readily extract the correlators (1).

We describe our system using the $t–J$ model[21], which is given by

$$H = \sum_{\langle ij \rangle} t(1 - \hat{n}_{i\bar{\sigma}})c^{\dagger}_{i\sigma}c_{j,\sigma}(1 - \hat{n}_{j\bar{\sigma}}) + J\left(\hat{\mathbf{S}}_i \cdot \hat{\mathbf{S}}_j - \frac{\hat{n}_i\hat{n}_j}{4}\right), \quad (2)$$

where $\bar{\sigma} = -\sigma$ denotes fermion spin. The $t–J$ model is an effective representation of the Hubbard model, which is realized in the experiment[18], that accurately captures low-energy physics at large onsite repulsion and is relevant for a doped Mott insulator. We set the super-exchange to $J/t = 0.3$, corresponding to an energy scale of the contact interaction given by $U/t = 4t/J \approx 13.33$. This
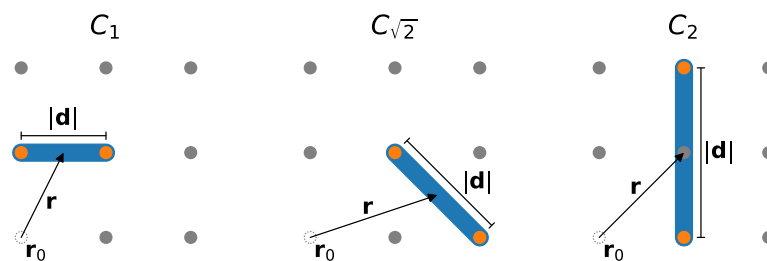

Fig. 1 Spin correlators. Illustration of C_1, $C_{\sqrt{2}}$, and C_2 which are defined in Eq. (1). Here, the bond distance $\mathbf{r}$ is defined as the distance from the carrier to the point between the spins for which the correlation is considered.
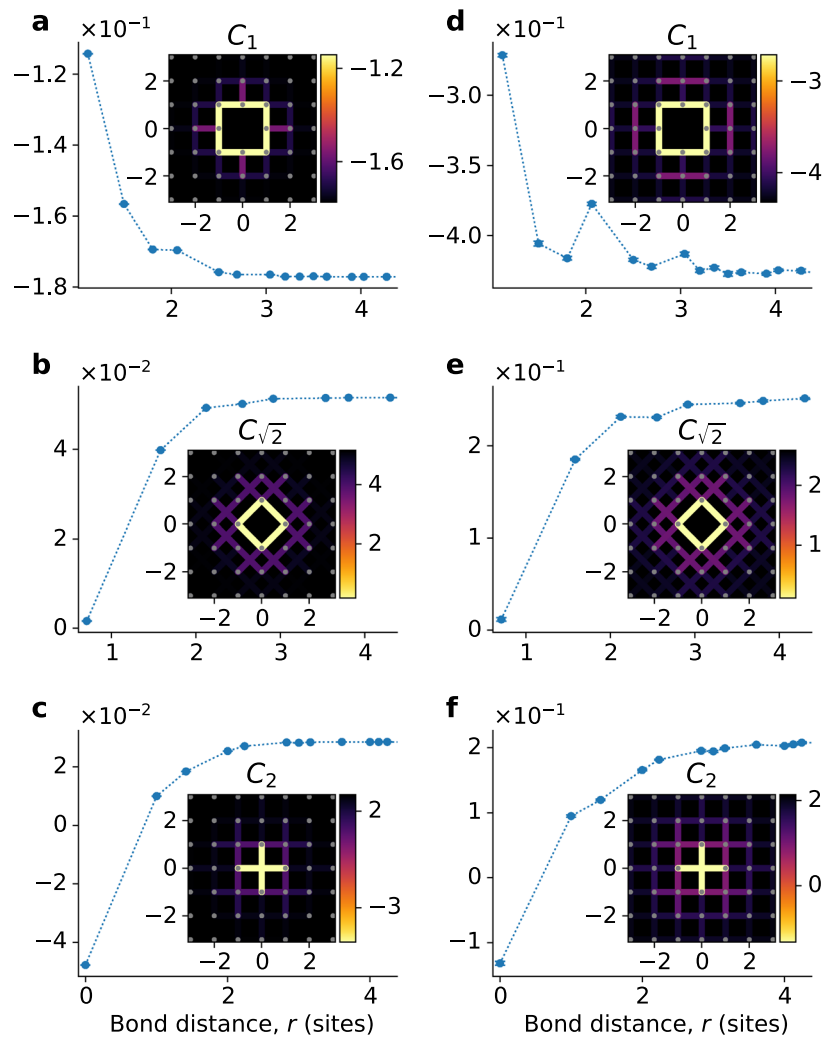
Fig. 2 Real-space structure of the polaron. Spin correlations as a function of the bond distance, obtained for a system with 20 × 20 lattice sites and periodic boundary conditions. The inset shows a top view of the lattice with spin correlations illustrated by the bond color. Here, $J/t = 0.3$ where J is the super-exchange parameter, and t is the hopping integral. This corresponds to $U/t \approx 13.33$ in the Hubbard model, where U is the onsite repulsion. Temperatures are given by $T = t/2.2$ (**a–c**) and $T = t/8.8$ (**d–f**) respectively. The nearest-neighbor correlations (**a**, **d**) reveal a reduction of anti-ferromagnetism, though the lack of ferromagnetism implies no significant increase in the mean-free path. Next-nearest-neighbor correlations (**b**, **e**) vanish near the carrier, implying a high degree of frustration that persists to low temperature. The combination of super-exchange and delocalization gives rise to anti-correlation across the carrier (**c**, **f**). Error bars correspond to one standard deviation.

parameter choice is directly comparable to the experiment[18], and puts us well into the strongly correlated regime.

Spin correlations. Using WAMC, we obtain spin correlators of the form (1). In Fig. 2a–c we display results at a temperature corresponding to $T = t/2.2$, which lies within the error bars of the experiment[18]. Like that work, we find a reduction of C_1 (a) near the carrier, though substantial anti-ferromagnetism persists even in its direct vicinity. The effect on $C_{\sqrt{2}}$ (b) is more dramatic than on C_1, with correlations virtually disappearing at $r = \sqrt{1/2}$. By comparison, experimental findings even indicate anti-correlation close to the carrier. For C_2, we find a dramatic reversal, with strong anti-correlation appearing across the carrier (c), in line with observations. Most likely this effect results from delocalization of the carrier: Moving the hole one lattice spacing brings two spins situated at opposite sides of the carrier into direct contact, where the interaction is antiferromagnetic. A comparison of theoretical and experimental results thus reveals a qualitative agreement with regard to the structure of the polaron. Some

quantitative differences persist, either as a result of discrepancies between the Hubbard and t–J models, or due to the experimental protocol applied in ref. [18]. We also find qualitative agreement with zero-temperature calculations based on DMRG and trial wave-function methods[23].

Reducing the temperature by a factor 4 (Fig. 2d–f), the magnitude of the spin correlations increases significantly, with background values of C_1 approaching the ground state value of an undoped system[24]. The spatial extent of the cloud of perturbed spins grows somewhat, while the basic features of its internal structure persist.

The reversal of C_2 and the reduction of $C_{\sqrt{2}}$ result from competing super-exchange processes that are activated as the carrier moves through the background. When the dopant hops a lattice spacing, spins that were previously next-nearest neighbors or situated on opposite sides of the hole—and therefore correlated —are brought in direct contact where the interaction is antiferromagnetic. From Fig. 2b, e, it is clear that this leads to a highly frustrated state with almost vanishing correlations that also persist at low temperatures.
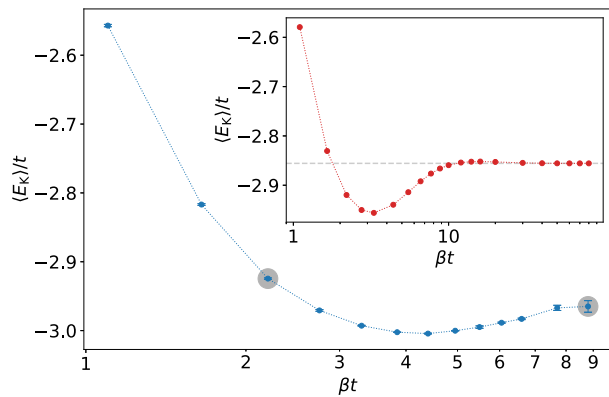
Fig. 3 Kinetic energy. The kinetic energy of the polaron is shown as a function of the inverse temperature in units of the hopping integral t. At lower temperatures, magnetic correlations build up in the background, increasing the energy cost of delocalizing the carrier. This is reflected in the non-monotonic dependence of kinetic energy on temperature. The inset shows kinetic energy for a 4×4 system, obtained via exact diagonalization. The parameter values used in Fig. 2 are indicated by gray discs. Error bars correspond to one standard deviation.

Kinetic energy. The spin configuration of the polaron does not reveal any ferromagnetic correlations, as is expected to occur in the limit $U \to \infty$[25]. Correspondingly, there is no significant increase in the mean-free path of the carrier, and its motion is only ballistic on short timescales[6]. Calculations carried out in the approximation of a dynamically passive background indicate that this translates to a suppression of the density of states at the band ends[4]. The resulting correlations thus indicate competition between super-exchange and processes that also involve propagation of the carrier. Purely kinetic mechanisms that drive the system towards ferromagnetism and an increased mean-free path are not visible in these data. This picture is further corroborated by the kinetic energy of the polaron, which is shown in Fig. 3. The frustration which is visible in Fig. 2b, e becomes increasingly important at low temperatures where the system develops strong magnetic correlations. This makes delocalization of the carrier energetically expensive, and below a threshold corresponding to $T/t \approx 2.3$, the kinetic energy increases with decreasing temperature.

Discussion

We present unbiased high-precision results for the real-space structure of a polaron in the t–J model. Our results reveal a distorted background that is characterized by reversal or depletion of spin correlations near the carrier, which is indicative of competing magnetic processes and frustration. We find a good agreement with recent quantum gas microscopy experiments, with minor discrepancies suggesting slight differences between our model and the physical system realized in ref. [18]. We have thus reached a point where direct comparison of experiments with single-site precision measurements and essentially approximation-free theoretical techniques is possible. With access to temperatures significantly below currently published experimental results, we can reach the regime where short-range correlations in the background approach ground state values for an undoped system. At the next stage, WAMC can be used to compute correlations between pairs of carriers, thereby providing critical insights into the temperature and energy scale of pairing. This can be carried out in tandem with experiments on multi-polaron structure formation in ultra-cold atomic gases, which have now become possible[26].

Methods

In our simulations, we represent fermions as world lines in space and imaginary time. We apply periodic boundary conditions with a lattice size of 20×20, which substantially exceeds the characteristic size of the polaron, ensuring that boundary pressure is not present. Periodic boundary conditions are also implemented in the imaginary-time direction, reflecting that the trace only involves diagonal elements of the density matrix. We use separate worms for the spin and charge sectors[19]. The former can wind in imaginary time, which alters the total spin in the system so that this sector is in the grand canonical ensemble. The worm corresponding to charge cannot wind, keeping the number of carriers to unity at all times. We confirm the accuracy of this technique by comparison to ED on a 4×4 lattice, see Supplementary Figs. 1 and 3.

In this setup, the sign problem appears as fermions may swap positions through a combination of hopping and super-exchange processes in the background. The first process which gives a sign change is of the order $t^2 J^3$, and becomes apparent at temperatures of $T/t \sim 0.5$. Relying on WAMC, we are able to resolve temperatures down to $T/t \approx 0.11$ with virtually vanishing error bars. The signal-to-noise ratio as a function of temperature is given in Supplementary Fig. 2. For further details about the sign problem in WAMC, see the Supplementary Methods.

Data availability

The data are available at https://github.com/emilbl/WAMC_tJ_1 with https://doi.org/10.5281/zenodo.3893046.

Code availability

The source code is available at https://github.com/emilbl/WAMC_tJ_1 with https://doi.org/10.5281/zenodo.3893046.

References

1. Lee, P. A., Nagaosa, N. & Wen, X.-G. Doping a Mott insulator: physics of high-temperature superconductivity. *Rev. Mod. Phys.* **78**, 17–85 (2006).
2. Alexandrov, S. & Devreese, J. T. *Advances in Polaron Physics* (Springer-Verlag, Berlin, Heidelberg, 2010).
3. de Gennes, P. G. Effects of double exchange in magnetic crystals. *Phys. Rev.* **118**, 141–154 (1960).
4. Brinkman, W. F. & Rice, T. M. Single-particle excitations in magnetic insulators. *Phys. Rev. B* **2**, 1324–1338 (1970).
5. Kane, C. L., Lee, P. A. & Read, N. Motion of a single hole in a quantum antiferromagnet. *Phys. Rev. B* **39**, 6880–6897 (1989).
6. Carlström, J., Prokof'ev, N. & Svistunov, B. Quantum walk in degenerate spin environments. *Phys. Rev. Lett.* **116**, 247202 (2016).
7. Trugman, S. A. Interaction of holes in a Hubbard antiferromagnet and high-temperature superconductivity. *Phys. Rev. B* **37**, 1597–1603 (1988).
8. Anderson, P. W. The resonating valence bond state in La₂CuO₄ and superconductivity. *Science* **235**, 1196–1198 (1987).
9. Schrieffer, J. R., Wen, X. G. & Zhang, S. C. Dynamic spin fluctuations and the bag mechanism of high-T_c superconductivity. *Phys. Rev. B* **39**, 11663–11679 (1989).
10. White, S. R. & Scalapino, D. J. Hole and pair structures in the t-j model. *Phys. Rev. B* **55**, 6504–6517 (1997).
11. White, S. R. Density-matrix algorithms for quantum renormalization groups. *Phys. Rev. B* **48**, 10345–10356 (1993).
12. Brunner, M., Assaad, F. F. & Muramatsu, A. Single-hole dynamics in the t-J model on a square lattice. *Phys. Rev. B* **62**, 15480–15492 (2000).
13. Loh, E. Y. et al. Sign problem in the numerical simulation of many-electron systems. *Phys. Rev. B* **41**, 9301–9307 (1990).
14. Carlström, J. Diagrammatic Monte Carlo procedure for the spin-charge transformed hubbard model. *Phys. Rev. B* **97**, 075119 (2018).
15. Carlström, J. Spin-charge transformation of lattice fermion models: duality approach for diagrammatic simulation of strongly correlated systems. *J. Phys. Condens. Matter* **29**, 385602 (2017).
16. Gross, C. & Bloch, I. Quantum simulations with ultracold atoms in optical lattices. *Science* **357**, 995–1001 (2017).
17. Mazurenko, A. et al. A cold-atom Fermi-Hubbard antiferromagnet. *Nature* **545**, 462–466 (2017).
18. Koepsell, J. et al. Imaging magnetic polarons in the doped Fermi-Hubbard model. *Nature* **572**, 358–362 (2019).
19. Prokof'ev, N. V., Svistunov, B. V. & Tupitsyn, I. S. Exact, complete, and universal continuous-time worldline Monte Carlo approach to the statistics of discrete quantum systems. *J. Exp. Theor. Phys.* **87**, 310–321 (1998).

20. Capogrosso-Sansone, B., Prokof'ev, N. V. & Svistunov, B. V. Phase diagram and thermodynamics of the three-dimensional bose-hubbard model. *Phys. Rev. B* **75**, 134302 (2007).
21. Chao, K. A., Spałek, J. & Oleś, A. M. Canonical perturbation expansion of the hubbard model. *Phys. Rev. B* **18**, 3453–3464 (1978).
22. Mishchenko, A. S., Prokof'ev, N. V. & Svistunov, B. V. Single-hole spectral function and spin-charge separation in the *t-J* model. *Phys. Rev. B* **64**, 033101 (2001).
23. Grusdt, F., Bohrdt, A. & Demler, E. Microscopic spinon-chargon theory of magnetic polarons in the *t−J* model. *Phys. Rev. B* **99**, 224422 (2019).
24. Khatami, E. & Rigol, M. Thermodynamics of strongly interacting fermions in two-dimensional optical lattices. *Phys. Rev. A* **84**, 053611 (2011).
25. Andreev, A. F. Structure of vacancies in solid He^3. *Sov. J. Exp. Theor. Phys. Lett.* **24**, 564–565 (1976).
26. Chiu, C. S. et al. String patterns in the doped hubbard model. *Science* **365**, 251–256 (2019).

Acknowledgements

Author contributions

Simulations were carried out by E.B. The paper was written jointly by E.B. and J.C.

Competing interests

The authors have no competing interests.

Additional information

Supplementary information is available for this paper at https://doi.org/10.1038/s42005-020-00408-z.

Correspondence and requests for materials should be addressed to J.C.

Reprints and permission information is available at http://www.nature.com/reprints.

Publisher's note Springer Nature remains neutral with regard to jurisdictional claims in published maps and institutional affiliations.